Title

Reverse-topology membrane scission by the ESCRT proteins

Journal

Nature Reviews Molecular Cell Biology, 18(1)

ISSN

1471-0072

Authors

Schöneberg, Johannes

Lee, Il-Hyung

Iwasa, Janet H

et al.

Publication Date

2017

DOI

10.1038/nrm.2016.121

Peer reviewed

HHS Public Access

Author manuscript

Nat Rev Mol Cell Biol. Author manuscript; available in PMC 2017 July 01.

Published in final edited form as:

Nat Rev Mol Cell Biol. 2017 January ; 18(1): 5–17. doi:10.1038/nrm.2016.121.

Reverse-topology membrane scission by the ESCRT complexes

Johannes Schöneberg[1,*], **Il-Hyung Lee**[1,*], **Janet H. Iwasa**[2], and **James H. Hurley**[1,3]

[1]Department of Molecular and Cell Biology and California Institute for Quantitative Biosciences, University of California, Berkeley, Berkeley, CA 94720, USA

[2]University of Utah, Salt Lake City, UT 84112, USA

[3]Molecular Biophysics and Integrated Bioimaging Division, Lawrence Berkeley National Lab, Berkeley, CA 94720, USA

Preface

The narrow membrane necks formed during viral, exosomal, and intra-endosomal budding from membranes, cytokinesis, and related processes have interiors that are contiguous with the cytosol. The severing of these necks involves action from the opposite face of the membrane as compared to the well-characterized coated vesicle pathways, and is referred to as “reverse” or “inverse” topology membrane scission. This process is carried out by the endosomal sorting complexes required for transport (ESCRT) proteins. In particular, the ESCRT-III proteins can form filaments, flat spirals, tubes and conical funnels, which are thought to somehow direct membrane remodeling and scission. Their assembly, and their disassembly by the ATPase VPS4, has been intensively studied, but the mechanism of scission has been elusive. New insights from cryo-electron microscopy and various types of spectroscopy may finally be close to rectifying this situation.

Introduction

Vesicular transport is central to eukaryotic cells, and it requires the continual fission and fusion of membranes. Vesicles can bud towards or away from the cytosol. The directionality of the budding, and subsequent scission, of vesicles is all-important both for the biological outcome and for the physical mechanism of their formation. Entirely different physical mechanisms govern scission of vesicles that bud towards or away from the cytosol. The endosomal sorting complexes required for transport (ESCRT) direct the scission of vesicles that bud away from the cytosol, whether into internal compartments or out of the cell (Fig. 1a). The scission of membrane necks from the outer surface can occur via constriction, as in ‘normal’ membrane scission. It is less obvious how reverse topology scission is directed from the inner surface.

The ESCRT proteins were discovered as factors required for the biogenesis of multivesicular bodies (MVBs). MVBs are endosomes that contain intraluminal vesicles (ILVs), which are formed when parts of the limiting membrane bud into the lumen of the endosome. Here, “limiting membrane” refers to the “main” outer membrane that delimits the endosome. The

Correspondence should be addressed to J. H. H. (jimhurley@berkeley.edu).
*Equal contribution

nascent ILVs are connected to the limiting membrane by a narrow membrane neck, which must be cut to release them into the lumen. The functions of the ESCRTs extend far beyond their role in MVB formation, however. In MVB biogenesis, the ESCRTs drive both budding and scission of ILVs. In many pathways, factors other than the ESCRTs drive the formation of the membrane neck, and the role of the ESCRT is limited to membrane scission. Indeed, it is reverse topology scission that is the hallmark of most ESCRT functions. Pathways that require the ESCRTs include the budding and release of HIV-1 and other viruses from host cells[1]; cytokinesis[2]; biogenesis of microvesicles and exosomes; plasma membrane wound repair; neuron pruning; extraction of defective nuclear pore complexes; nuclear envelope reformation; plus-stranded RNA virus replication compartment formation[3–5]; and micro- and macroautophagy[5] (Fig. 1b). Here, we focus on the mechanism of membrane scission by the ESCRTs, while leaving the biological functions of the ESCRTs to other reviews[3–5].

The ESCRT machinery

The core ESCRT machinery consists of the ESCRT-I, ESCRT-II and ESCRT–III complexes, ALIX (also known as BRO1 or PDCD6IP) and VPS4 (Table S1). ESCRT-I and ALIX bind various pathway-specific signals that recruit ESCRTs to their sites of action. In MVB biogenesis, for example, the main pathway-specific signal is ubiquitin, which binds to ESCRT-I, ESCRT-II, and ALIX[6]. ESCRT-III proteins exist as soluble monomers in solution. When activated by membrane-associated ESCRT-II or ALIX, ESCRT-III assembles on membranes into filamentous structures of variable morphology, composition and stoichiometry. These ESCRT-III assemblies are thought to be the main drivers of membrane remodeling and scission. ESCRT-III disassembly requires the action of the final core ESCRT component, the hexameric AAA+ ATPase VPS4.

ESCRT-I-II

ESCRT-I-II recruits, activates, and orchestrates the ESCRT-III-dependent scission process, hence an understanding of their structure and function is indispensable. The ESCRT-I complex[7] is a stalk-shaped heterotetramer of TSG101 (Vps23 in yeast), VPS28, VPS37A-D, and one of MVB12A, MVB12B or UBAP1[8]. ESCRT-II[9] is a Y-shaped heterotetramer containing one copy of VPS22 (also known as EAP30) and VPS36 (also known as EAP45), and two of VPS25 (also known as EAP20)[10–12]. The C-terminal domain of the VPS28 subunit of ESCRT-I is the locus for ESCRT-II recruitment[13, 14], which connects the two via the VPS36 subunit of ESCRT-II[15]. In solution, yeast ESCRT-I-II assemble into a 1:1 supercomplex. The supercomplex is flexible; it can fold itself up such that it spans just 210 Å, or extend to 380 Å[15]. The latter distance exceeds the diameter of one of the yeast ILVs generated by the ESCRTs, illustrating how the molecular and organellar size scales converge in the analysis of this system.

The ESCRT-I and –II complexes comprise the first branch of a two-pronged pathway for recruitment of ESCRT-III to scission sites (Fig. 2). The high affinity of ESCRT-I and -II for one another[14, 15] and findings from *in vitro* reconstitutions[16, 17] have suggested that these complexes are obligate partners. However, knockdowns of ESCRT-II subunits on their own has no effect on cytokinesis[18] or HIV-1 release[19]. On the other hand, various imaging,

reconstitution, and overexpression studies had implicated ESCRT-II in cytokinesis[20] and HIV-1 release[17, 21]. It is now clear, based on a study using multiple knockdowns, that ESCRT-II has a direct role in cytokinesis[22]. The chain of interactions involved is identical to that established by structural and reconstitution studies. The difficulty in establishing a role for ESCRT-II in cytokinesis was redundancy between ESCRT-I and/or ESCRT-II and ALIX, which mediates a second branch of the pathway (Fig. 2). It seems that the role of ESCRT-II in HIV-1 release has probably also been obscured by redundancy between the pathways. These data show that in mammalian cells ESCRT-I -II and ALIX comprise two partially redundant entry points to ESCRT-mediated membrane scission in MVB biogenesis, HIV-1 release, and cytokinesis. Moreover, this also appears to be true in yeast MVB biogenesis[23].

ESCRT-I and –II complexes colocalize at the necks of buds reconstituted in giant unilamellar vesicles (GUVs)[16]. Structures of “struts” corresponding to ESCRT-I-II have been visualized in electron micrographs of the plasma membranes of cells[24, 25] (Fig. 3a). The curvature of rim of the membrane neck is neither net negative or positive, and is referred to as “saddle-shaped” instead given that it is simultaneously negative with respect to one axis and positive with respect to another. Theoretical modeling of the energetics of membrane budding suggests that their ability to form a saddle-shaped protein assembly is important[26, 27]. This is because the neck of the membrane bud is convex with respect to one axis and concave with respect to the other. Therefore any protein complex involved in stabilizing the neck needs to have complementary concave and convex surfaces.

The Y-shape of the ESCRT-II complex results in two ESCRT-III binding sites at the ends of two of the three branches of the Y, and both are essential for function in MVB biogenesis[10, 28]. The crystal structure of the human ESCRT-II subunit VPS25 WH2 domain bound to a fragment of ESCRT-III subunit charged multivesicular body protein 6 (CHMP6) led to a model in which ESCRT-II and CHMP6 together form a curved complex[29] (Fig. 3b). The ESCRT-II–$CHMP6_2$ complex has a convex basic face complementary to a concave acidic membrane[29]. This could contribute to the nucleation of ESCRT-III filaments as described in depth below.

ALIX

ALIX (Bro1 in yeast)[30, 31] represents an alternative to the ESCRT-I-II complex for ESCRT-III recruitment and activation. ALIX consists of a Bro1 domain[32], V domain[33, 34], and proline-rich domain (PRD), and functions as a homodimer[35]. The main function of the curved Bro1 domain is to bind to the C-terminal helix of ESCRT-III protein CHMP4 at a site on its concave face[32, 36]. The central V domain binds to viral and cargo sequences and to ubiquitin[37–39]. The C-terminal PRD binds to upstream elements and other ESCRTs, and autoinhibits the V domain[40]. ALIX dimerizes via its V domain[35], thus it resembles ESCRT-II in having two ESCRT-III binding sites on its outer arms (Fig. 3c). HD-PTP is an ALIX-like protein that also contains a tyrosine phosphatase domain. In some contexts HD-PTP can replace ALIX in recruiting CHMP4[41–43].

ESCRT-III

The ESCRT-III complex is most immediately involved in reshaping and severing membranes. As such it has been center-stage in mechanistic research. In humans, these are the charged multivesicular body (CHMP) proteins 1–7 (CHMP1A/B, also known as Did2 in yeast; CHMP2A/B, also known as Vps2 in yeast;CHMP3, also known as Vps24 in yeast; CHMP4A/B/C, also known as Snf7 in yeast; CHMP5, also known as Vps60 in yeast; CHMP6, also known as Vps20 in yeast; and CHMP7, also known as Chm7 in yeast) and increased sodium tolerance-1 (IST1) (Fig. 4a). High resolution structures are available for CHMP3[44], CHMP4[45], IST1 and CHMP1B[46–48] (Fig 4b). The ~100 N-terminal residues form an electropositive and rigid two-helix hairpin (helices α1–α2). These electropositive regions have the main contacts with membranes. The four shorter helices (α3–α6) that follow are electronegative. The more N-terminal portions (α1–α4) seem to be the main structural components of ESCRT filaments, as described below, while the C-terminal helices (α5 and α6) serve regulatory roles.

Many of the ESCRT-III proteins change their conformation dramatically in the course of their functions. This was first noticed in an analysis of C-terminal truncations of ESCRT-III proteins. Truncating helix α5 of various ESCRT-III proteins promotes their assembly, apparently by promoting access to a conserved region of the α1–α4 core[49, 50]. When α5 is folded back onto α1–α4, this state is referred to as the closed conformation (Fig. 4b). In addition to truncation, α5 can also be artificially displaced from its binding region in vitro by increasing the salt concentration[51]. This can be also achieved by point mutations such as Snf7 Arg52Glu[52], which presumably destabilize the connection between the α1–α4 core and α5.

Small angle x-ray scattering (SAXS)[51, 53, 54] provided the first direct physical evidence for the ESCRT-III conformational change in solution, albeit at low resolution. Now, a high resolution cryo-electron microscopy (cryo-EM) structure of the IST1–CHMP1B copolymer[48] (Fig 4b) and a crystal structure of helices α1–α4 of CHMP4[45] (Fig. 4b) reveal that opening of ESCRT-III involves even larger changes than anticipated. In both the CHMP1B and CHMP4 structures, helices α2 and α3 are melded into a single helix, extending the α1–α2 hairpin. Previously unstructured regions join helix α4, extending it as well. Thus, opening involves the complete reorganization of about half of the monomer structure.

The IST1–CHMP1B polymer structure revealed that IST1 comprises the outside of the tube and CHMP1B the inside. IST1 is in the closed conformation, which was a surprise in that it had been expected that all assembled ESCRT-III proteins would be in the open state. This structure shows that this is only necessary for a subset of the subunits. The open CHMP1B is, if anything, even more open than had been expected. The CHMP1B is so elongated that it spans the i^{th} to $i+4^{th}$ molecule of IST1. It seems likely that the open conformation is the one that is relevant for membrane binding. Even though the crystal structure of the N-terminal part of CHMP4 is now known in an open conformation, it is still difficult to make inferences about how this and other open-conformation ESCRT-III subunits bind to membranes. It remains critically important to determine the atomic resolution structures of some of the

"conventional" reverse-topology ESCRT-III assemblies described below, ideally in the presence of membranes.

Structural basis of ESCRT-III assembly

ESCRT-III carries out all of its known functions in the context of membrane-bound assemblies. Yet in the absence of activating and recruiting signals, ESCRT-III subunits reside as inert monomers in the cytosol. The diversity of the forms and structures into which ESCRT-III subunits can polymerize is rich and comprises spirals, tubes, coils and cones (Fig. 5). Here we will describe the morphologies, but defer slightly the discussion of their mechanistic implications. The full spectrum of these structures is at the heart of the most up-to-date mechanistic hypotheses, as described below under "scission mechanism".

Spirals

Flat ESCRT-III spirals were first observed by deep etch EM (DEEM) microscopy of the plasma membranes of cells overexpressing CHMP4[55] (Fig. 5a). This observation was replicated *in vitro* with the yeast and *C. elegans* orthologs[52, 56, 57]. *C. elegans* CHMP4 spirals consist of 4.2 nm-filaments[56] or a mixture of 4.9nm and thicker 10.6nm filaments. C-terminally truncated CHMP2A also forms spirals[58, 59]. In isolation, CHMP4 growth is not self-limiting, and spirals will grow until all the available space is occupied or the soluble pool is depleted.

CHMP4 filaments have a preferred radius of curvature of 21–32 nm[56, 57]. Their innermost observed ring is slightly overbent (18 nm), meaning that the coils are bent at a higher curvature than their natural energy minimum. Meanwhile, the outer rings are underbent, meaning that their radii of curvature are greater (i.e. less curved) than the preferred value[56, 57]. Molecular dynamics simulations[56] and atomic force microscopy (AFM) measurements[57] arrived at persistence lengths of 800 and 260 nm, respectively. AFM is invaluable in this context because of its ability to not only visualize assemblies, but also to apply force to them and to sever filaments. CHMP4 filaments are ~5-fold stiffer than DNA, but ~15-fold softer than actin. This suggests that CHMP4 filaments are stiff enough to act as mechanical springs.

Tubes

Tubular evaginations of ESCRTs were first observed in the same seminal DEEM study of CHMP4-overexpressing cells[55]. Evaginations are ~100–120 nm in diameter and extend to varying heights. Overexpression of CHMP2B also leads to evaginations of up to 400 nm in diameter[60]. Heteropolymeric CHMP2A-CHMP3 tubes[58] are ~50 nm in diameter and have a repeating unit of ~4 nm[59] (Fig. 5b). The outer surface of these tubes binds membranes, while the inner surface provides access to Vps4[58]. This topology fits with the function of ESCRTs in reverse-topology scission. The IST1-CHMP1B combination also forms a heteropolymeric tube, with a 24-nm diameter and 5.1-nm repeat, and has yielded a cryo-EM reconstruction at atomistic resolution[48] (Fig. 5c). Formation of tubes of a range of diameters thus appears to be a widespread property of ESCRT-III proteins.

The biggest surprise in the IST1-CHMP1B structure[48] was that the outer surface, which had been expected to bind to membranes, was highly electronegative and so incompatible with binding to acidic phospholipids. The lumen of the tube, in contrast, was electropositive. This led to the insight that the IST1-CHMP1B pair can coat the positively curved outside of tubular vesicles in a “normal” topology. BAR domain proteins, a well-established family of banana-shaped proteins involved in “normal” topology membrane tubulation and scission, also coat membranes in this way[48]. Cell studies have now confirmed that IST1 and CHMP1B sever normal topology membrane tubes[48, 61]. This discovery raises a host of questions. IST1 and CHMP1B are known to be present at sites of reverse-topology scission, but it is not clear how the structure of their co-polymer could participate in such reactions. This begs the question as to the structures of IST1 and CHMP1B when alone or combined with other ESCRTs at sites of reverse topology scission. It is hard to see how normal topology scission by IST1 and CHMP1B could simply be a mirror image of reverse-topology scission, and it will be important to explore what the relationship is between the two processes.

Cones and Coils

Tubular ESCRT assemblies cannot extend indefinitely when surrounded by lipids, and must close at one end[55]. In vitro co-assembly of CHMP2A and CHMP3 showed these closures consist of cones and domes of 25 nm height on top of 50 nm diameter tubes[58]. Later studies revealed much wider cones for both CHMP2/CHMP3 hetero- and even CHMP1B homopolymers. Such cones tapered from 150 nm diameter to 50 nm in diameter, displaying evidently non-equivalent radial contacts[62]. Similar cones, based on a 17 nm-filament, were seen in cells during cytokinetic abscission[63]. A distinctive feature of these filaments is the large filament-filament distance of 35 nm as opposed to the tight packing of, for example, CHMP2/CHMP3 tubes of 3.5 nm spacing. CHMP2-CHMP3 also form “slinkies”[52, 58] (Fig. 5d, ii and iv), by which we mean helical structures with large gaps between subsequent turns of the helix.

Kinetic basis of ESCRT assembly

ESCRT assembly is highly ordered and exquisitely choreographed. Understanding the temporal basis for assembly is as important as the spatial basis. HIV-1 budding and cytokinesis have been useful models for the kinetics of ESCRT assembly. In both cases, the fusion of fluorescent tags to ESCRT-III subunits interferes with function. Careful controls must be carried out to validate that tagged ESCRT-III subunits are expressed at low levels relative to endogenous subunits, and are not acting as dominant negatives.

HIV-1 budding is driven by the assembly of a single viral protein, Gag. Nascent HIV-1 particles steadily accumulate Gag for ~10 min[64, 65] prior to scission. ESCRT-I is recruited to HIV budding sites in parallel with Gag[65]. In contrast, CHMP4B and VPS4 are recruited in shorter bursts during the final phase of Gag assembly[65]. The mere presence of ESCRT-I is thus insufficient to recruit CHMP4B. In cytokinesis, ESCRT proteins help sever the intercellular bridge[18, 66, 67]. Over the course of this ~120 min process, the protein CEP55 localizes to the midbody during the first 0–40 min, followed by ESCRT-I at 40–80 min[68].

CHMP4B is recruited in two pulses, the first at 40–80 min, and a second at 80–120 min[68]. The second pulse is thought to correspond to abscission[68]. The second pulse of CHMP4 in cytokinesis probably corresponds to the scission-active pool seen in HIV-1 release.

In vitro reconstitution systems allow ESCRT kinetics to be measured precisely in a controlled environment. Recent studies have measured the kinetics of CHMP4B polymerization[57, 69], a central step in membrane scission. Nucleation is defined as the kinetic step in which an initial seed unit is assembled that once formed, can readily grow into a larger structure. *In vitro* analysis using negatively curved supported lipid bilayers created by nanofabrication showed that CHMP4B nucleates much faster on negatively curved membranes[69]. CHMP4B nucleation is also accelerated by the presence of ESCRT-II and CHMP6[69]. In contrast, CHMP4B polymer growth is independent of both membrane curvature and upstream activators. Once the nucleation barrier is overcome, purified CHMP4 seems able to grow indiscriminately until the supply runs out or something else halts it. In cells, capping by CHMP2 and CHMP3 seems to be responsible for preventing uncontrolled CHMP4 polymerization[70] via a mechanism that is still unclear.

Vps4: The recycling machine

There is a consensus that VPS4[71, 72] has an essential role in recycling ESCRT-III subunits, but is probably does more than that. The questions surrounding the precise role of VPS4 are at the crux of much of the uncertainty about how ESCRTs actually sever membranes. Before these questions can be answered, it is essential to understand how VPS4 extracts ESCRT-III monomers from the assembly. There has been major progress on this front, which we discuss next.

Vps4 consists of an N-terminal microtubule interaction and transport (MIT) domain[73] and a catalytic AAA+ ATPase domain[72]. Similarly to many other AAA+ ATPases, Vps4 functions as a hexamer[74, 75]. The established recycling function of Vps4 depends on the interaction of the MIT domain with MIT-interaction motifs (MIMs) in ESCRT-III subunits. MIT domains consist of three helix bundles that interact with protein partners through multiple interfaces. The canonical interaction of ESCRT-III with the Vps4 MIT domain occurs through the MIM1 of the ESCRT-III subunits CHMP2B (Vps2 in yeast)[76, 77], CHMP1A[77] and IST1[78]. The MIM1 consists of a single α-helix that interacts with helices α2 and α3 of the Vps4 MIT domain through several key Leu residues of MIM1. MIM1 obeys the consensus sequence (D/E)*XX*L*XX*RL*XX*L(K/R). A different interaction is formed between the extended-conformation MIM2 of the ESCRT-III subunit CHMP6 and helices α1 and α3 of Vps4 MIT[79]. CHMP4 and CHMP5 also interact with Vps4-MIT through MIM2 motifs, but with affinities in the range of hundreds of μM, as compared to low μM for CHMP6. CHMP3 has no Vps4-interacting MIM; however, CHMP3 and most other ESCRT-III subunits have sequences that bind to a range of other MIT domains from the Vps4 cofactor LIP5 (also known as Vta1 in yeast)[80, 81], the deubiquitylating enzymes UBPY (also known as USP8), AMSH (also known as STAMBP) and Doa4[82], and other proteins that are beyond the scope of this Review. Engagement of the MIT domain of VPS4 by MIM motifs potently activates ATP hydrolysis by the catalytic domain of VPS4[83–86].

Recently, a structure of an active, asymmetric hexamer has been determined, for the catalytic domain of Vps4 from *Metallosphera sedula*[75] (Fig. 6a). The structure confirms the presence of a central pore (see the center of the ring, right side view, Fig. 6a), as previously inferred from EM and modeling studies[87–91]. A Glu residue from pore loop 2 projects into the pore. ADP occupies one high affinity and five low affinity sites, whereas ATP seems to bind all six sites equally. While the presence of a central pore was inferred from the structures of other AAA+ proteins, a critical question has been what, exactly, was the function of the VPS4 pore. In one model, subunits of ESCRT-III were translocated through the center of the pore and released into solution on the opposite side of the ring. In another model, subunits remained folded and are released "in *cis*" with respect to the assembly. A disassembly study from our group using hydrogen-deuterium exchange and site-directed cross-linking resolved this question, and showed that ESCRT-III subunits are completely unfolded and translocate through the central pore of Vps4[92](Fig. 6b).

The outer tips of eukaryotic Vps4 proteins contain an insertion known as the β-domain. This domain interacts with the MIT-domain containing cofactor LIP5[87]. LIP5 contains a pair of tandem MIT domains at its N-terminus[81] that directly bind to ESCRT-III subunits. These contribute to increased avidity of ESCRT-III binding, increase the repertoire of subunits that can be bound, and transmit activation signals from ESCRT-III to VPS4[93]. LIP5 also contains a central linker and a C-terminal VSL domain that binds the VPS4 β-domain. The VSL domain is a constitutive dimer, and the dimer interface is essential for function[81]. The structure of the LIP5 VSL–VPS4 β-domain complex[94] led to a model in which a continuous network of LIP5 dimers connect a lattice of VPS4 hexamers.

Vps4 interacts with only some of the ESCRT proteins that contain MIM domains. CHMP1, CHMP2, CHMP6, and IST1 bind to Vps4 strongly, whereas other ESCRT proteins bind with low (CHMP4) or negligible (CHMP3) affinity[73, 79]. It is not yet clear how weakly interacting or non-interacting subunits of ESCRT-III are disassembled. One possibility is that the binding of "strong" ESCRT-III subunits to "weak" ones (where "strong" and "weak" refer to their Vps4 affinities) is tight enough that the strong subunit can feed the weak one into the translocation pore for disassembly. LIP5, which does bind tightly to some of the "weak" subunits, might help here. Another possibility is that once enough strong subunits are pulled out of the assembly, the remaining subunits simply fall apart, like bricks without mortar. Indeed, Vps4 only needs to unfold about half of the subunits in a model filament in order to disassemble the entire filament[92].

Scission mechanism

The experiments described above have told us much about how the ESCRTs arrange themselves in space and time. The overarching task now is to deduce how these arrangements lead to reverse-topology membrane scission. Here, we consider this from the point of view of HIV-1 release. The formation of the attached HIV-1 bud is independent of ESCRTs. In other pathways, this is not necessarily the case. In MVB biogenesis, for example, the ESCRTs promote both budding and scission. In cytokinesis the process is even more complex, and the ESCRTs seem to be involved in the massive narrowing of the cytokinetic neck from 1.5 μm all the way to zero.

Dome models

The dome model put forward by Kozlov and colleagues[95] was the first energetically detailed model proposed to explain membrane scission. This model was motivated by the experimental observation that ESCRT-III alone could sever otherwise empty membrane buds in a GUV system[96], and that the tips of lipid-coated CHMP2-CHMP3 copolymer tubes seemed to taper and close into a dome at one end[58]. In this model, the strong binding of the dome-shaped ESCRT-III polymer to the lipid membrane constricts the bud neck, and so leads to vesicle fission. Measurement of the protein-lipid interaction energy and comparison to the energy required for membrane deformation from elasticity theory showed that there is sufficient energy available to drive scission[95].

Video 1 (Supplementary information) and Fig. 7a show an elaboration of the dome model in action in HIV-1 release. In this and all other models of ESCRT-mediated HIV-1 release, Gag recruits ESCRT-III to the bud neck through ESCRT-I-II and ALIX. Subsequent to the original proposition of the dome model, conical structures have been directly visualized (see Fig. 5b, c, e), and the ESCRT-III assembly is shown as a pointed cone rather than as a rounded dome. The model shown in Video 1 includes the AAA+ ATPase VPS4, which was not part of the original dome model. VPS4 has consistently been imaged at HIV-1 bud necks[64, 65], leading to the view that its activity is required for HIV-1 release at a step prior to scission, not just for disassembly and recycling. In the model shown in video 1, the spontaneous growth and narrowing of the ESCRT-III cone would not in principle seem to need the presence of VPS4, and indeed, conical ESCRT-III structures can be produced *in vitro* from pure ESCRT-III proteins without the presence of VPS4[48]. One criticism of this version of the dome model is that it does not explain the presence of VPS4 prior to scission.

This model does explain the PALM microscopy observation of ESCRT proteins inside of budding HIV-1 virions, not only in the cytosol[97]. However, these observations have been challenged[98]. The prevailing view in the field is that most of the ESCRTs are released into the cytosol, not the virion. Indeed, release of ESCRTs into the virion would make this mechanism inconsistent with the mainstream view that in MVB biogenesis, the ESCRTs are recycled into the cytosol, not lost into intralumenal vesicles.

Several variations of the original dome model have been proposed. In one variant model, Vps4 pulls ESCRT-III subunits out of the polymer, thereby contracting the polymer[99]. However, this Vps4-dependent contraction through selective ESCRT-III subunit removal has not been observed. As cones have been shown to form in the absence of Vps4 and ATP[48], it is unclear why such a process would be needed. The biggest difficulty for the dome model as shown in video 1 comes from recent DEEM of ESCRT-III surrounding HIV-1 Gag assemblies in cells depleted of VPS4[24]. These images show a conical funnel of ESCRT-III filaments whose narrow end is in the Gag bud and whose wide end is on the cytosolic face of the plasma membrane (Fig. 5e), the opposite of the geometry in video 1.

Reverse dome model

The mechanism shown in Video 2 and Fig. 7b severs the membrane using the same type of constriction as in video 1, but acting from the opposite side of the bud neck. The model

shown in video 2 is compatible with the DEEM images[24] and with the prevailing view that the ESCRTs are released into the cytosol following severing. This mechanism has probably been the leading model in the field[100, 101]. One of the difficulties with this model is that the ESCRT proteins have to nucleate on the virion side of the bud, and ESCRT-III also has to taper to a point on the virion side. This would require the direction of the ESCRT-III cone to invert midway through its assembly (Video 2). Presumably this dramatic remodeling of the assembly would need to be actively guided in an ATP-dependent manner. Conceivably VPS4 could have this role, as shown in video 2.

Both the standard and reverse dome models have an additional inconsistency with experimental data. The dome models require that ESCRT-III filaments taper to a narrow tip, yet this would require CHMP4 filaments to spontaneously adopt an energetically unfavorable “overbent” conformation[57]. The observation, however, is that CHMP4 polymers nucleate at highly negatively curved regions of membranes[69], and then grow towards zones of lower rather than higher curvature.

Buckling models

A second category of ESCRT scission model involves mechanical buckling forces applied to the membrane by ESCRT-III filaments. The physical plausibility of membrane buckling induced by generic curved filaments was established several years ago[102], and has begun attracting more attention in the ESCRT field. Molecular dynamics calculations brought this principle to the case of a real ESCRT-III polymer[56]. The real-time observation of membrane buckling by CHMP4[57] has now given prominence to the buckling model. Buckling can directly give rise to membrane invaginations[57]. It is also possible for buckling to run in reverse and to lead to membrane scission[103], as shown at the end of Video 3 and in Fig. 7c. The latter idea depends on the presence of an excess of overbent CHMP4, which can only relax by flattening out.

The buckling or “spiral spring” model is shown in Video 3. The shape of the ESCRT-III funnel matches the DEEM images[24]. In this model, the conical structure nucleates where membrane curvature is negative[69] and grows from narrow to wide[57, 69]. One role of VPS4 here might be to remove the first ring of ESCRT-III and so untether the ESCRT-III assembly from HIV-1 Gag and upstream ESCRTs. Once untethered, overbent CHMP4 would be free to flatten out as shown in video 3. Another possibility is that VPS4 modulates the composition of ESCRT-III subunits. The copolymerization of CHMP2 and/or CHMP3 with CHMP4 favors three-dimensionally curved ESCRT-III coils[52]. VPS4 has a much higher affinity for CHMP2 than for CHMP4. In principle, the selective extraction of CHMP2 from a CHMP4–CHMP2 copolymer might lead to flatter structures, thereby releasing the energy stored in the deformed membrane and make it available to drive scission. This buckling model does not require the direction of cone growth to change, and it predicts the release of ESCRT-III subunits into the cytosol. In our view, the spiral spring/buckling model is currently the most plausible contender.

ESCRTs in endosomal cargo sorting

A major unsolved question in MVB biogenesis is how ubiquitylated cargoes are sorted into ILVs. In conventional vesicular traffic, transmembrane cargoes bind to adaptor complexes, which in turn bind to coat proteins such as clathrin[104, 105]. This provides a direct connection from cargo recruitment to vesiculation. In MVB biogenesis, the ESCRTs accumulate at the bud neck, while the cargo is packaged into the lumen. Thus the packaging elements and the cargo are physically separated from one another. The spiral spring/buckling concept described above breathes new life into the "concentric circle" model for cargo sorting[106]. Here, a cargo domain organized by ESCRT-0 accumulates within a peripheral ring of ESCRT-I and –II complexes. In turn it would become encircled by ESCRT-III. When first proposed, the model failed to explain how membrane deformation would be triggered, or how the ESCRT-I and –II complexes would avoid engulfment. In the spiral spring version of the concentric circle model (Video S4), the CHMP4 polymer grows such that filaments are underbent, leading to mechanical tension. Incorporation of additional types of ESCRT-III subunits such as CHMP2 might facilitate conversion into a three-dimensional helix, as seen for *in vitro* mixtures of the yeast proteins[52]. In the combined spiral spring/concentric circle model, deformation of the membrane would simultaneously release tension and drive the central cargo domain into the newly formed bud. The subsequent release of CHMP2, a favored substrate of VPS4, could drive the remaining CHMP4 back into a flat spiral, resulting in scission.

Conclusions and outlook

The exciting observations described over the past two years make one optimistic that we are within striking distance of a structural and biophysical explanation of the ESCRT mechanism. Highlights include the topology of ESCRT filaments emanating for HIV-1 Gag budding sites[24], spiral spring models for mechanical deformation of membranes[5657], and a high resolution cryo-EM reconstruction of a helical ESCRT co-polymer[48]. But triumphalism would be premature. Six to seven years ago, in the wake of the solution of the crystal structures of nearly all of the ESCRT components, and the reconstitution of substantial aspects of ESCRT function, it was tempting to speculate that "the mechanism" was in sight. Looking back on it last year, Odorizzi wrote that " Despite the assignment of activities performed by certain ESCRTs that was suggested *in vitro* many of the details about their operations remain fuzzy. Perhaps the wooliest thinking concerns ESCRT-III structure-function"[107]. The ESCRT-III proteins have tossed us myriad red herrings. They assemble into fascinating, sometimes beautiful, and sometimes messy structures *in vitro* or when overexpressed. Form follows function, but seeing too many forms at once can make it harder, not easier, to deduce function.

Nevertheless, we are once again having a hard time containing our optimism. The insights obtained even from the moderate resolution of the DEEM technique[24] are compelling, and its seems only a matter of time before their high-resolution cryo-em counterparts in cells or in reconstituted systems generate decisive insights. Indeed, we already have an atomistic image of a reconstituted ESCRT tube, albeit of the inside-out odd couple CHMP1B-IST1[48]. It will be fascinating to see what happens structurally if a "normal"-topology tube such as

CHMP2-CHMP3 met a CHMP4 spiral, for example. An appreciation of the mechanical nature of Snf7 filaments has been long overdue. These insights, coming first from simulations[56] and then from direct measurement by AFM[57], are, to pardon the expression, reshaping how we think about their ability to remodel membranes. Perhaps we are not so far away from combing, carding and weaving the “wooly thinking” into a shimmering fabric of insight.

Supplementary Material

Refer to Web version on PubMed Central for supplementary material.

Acknowledgments

ESCRT research in the Hurley lab is supported by the National Institutes of Health, grant AI112442. J. Iwasa is supported by the CHEETAH center, National Institutes of Health, grant GM082545.

Biographies

Joh Schöneberg received his Ph.D. from the Free University Berlin under the supervision of Frank Noé. For his postdoc he joined the labs of Gerhard Hummer at the Max Planck Institute of Biophysics in Frankfurt, Germany, and James H. Hurley at the University of California Berkeley, USA to combine theory and experiments. His current research is focused on membrane proteins, in particular the ESCRTs.

Il Hyung Lee is a postdoctoral researcher in the laboratory of James Hurley at the University of California, Berkeley, USA. He carried out his doctoral work with Jay Groves at the same institute. He studies molecular mechanism of membrane remodeling processes using membrane reconstitution and various imaging techniques.

Janet Iwasa is a faculty member in the Biochemistry Department at the University of Utah. Her broad goal is to create accurate and compelling molecular visualizations that will support research, learning and scientific communication

James Hurley is a professor at UC Berkeley and previously led a laboratory at the National Institutes of Health. He has contributed to many aspects of the structural biology of membrane-associated proteins in signal transduction, membrane traffic, protein degradation, and HIV biology. In particular, he is known for his structural and in vitro reconstitution studies of the ESCRT machinery.

Glossary

Cytokinesis
The separation of daughter cells, which is the final stage in cell division in which the membrane and microtubules connecting the two cells are severed

Membrane necks
Narrow membranous connections linking such entities as nascent endosomes, exosomes, enveloped viruses and intralumenal vesicles to their membranes of origin; daughter cell to

mother or daughter cell; cytosol to lumen of a double-membrane structure such as the nucleus or a nascent autophagosome

Reverse-topology scission
The severing of membrane necks when the scission factors function from the membrane face contiguous with the interior of the neck

Ubiquitin
A 76-amino acid protein whose covalent conjugation to target proteins can (among many other fates) mark them as substrates for the ESCRT system

Multivesicular body (MVB)
A late endosome containing internal vesicles

Giant unilamellar vesicles (GUVs)
Synthetic vesicles of ~5 to ~50 microns in diameter; a popular model system for *in vitro* studies of membrane remodeling

Gag
The structural protein of the HIV-1 capsid

Intercellular bridge
The narrow membranous and microtubule-containing structure connecting two daughter cells immediately prior to their separation in cytokinesis

References

1. Votteler J, Sundquist WI. Virus Budding and the ESCRT Pathway. Cell Host Microbe. 2013; 14:232–241. [PubMed: 24034610]
2. Martin-Serrano J, Neil SJD. Host factors involved in retroviral budding and release. Nature Reviews Microbiology. 2011; 9:519–531. [PubMed: 21677686]
3. Olmos Y, Carlton JG. The ESCRT machinery: new roles at new holes. Curr Opin Cell Biol. 2016; 38:1–11. [PubMed: 26775243]
4. Campsteijn C, Vietri M, Stenmark H. Novel ESCRT functions in cell biology: spiraling out of control? Curr Opin Cell Biol. 2016; 41:1–8. [PubMed: 27031044]
5. Hurley JH. ESCRTs are everywhere. EMBO J. 2015; 34:2398–2407. [PubMed: 26311197]
6. Shields SB, Piper RC. How ubiquitin functions with ESCRTs. Traffic. 2011; 12:1307–1317.
7. Katzmann DJ, Babst M, Emr SD. Ubiquitin-dependent sorting into the multivesicular body pathway requires the function of a conserved endosomal protein sorting complex, ESCRT-I. Cell. 2001; 106:145–155. [PubMed: 11511343]
8. Kostelansky MS, et al. Molecular architecture and functional model of the complete yeast ESCRT-I heterotetramer. Cell. 2007; 129:485–498. [PubMed: 17442384]
9. Babst M, Katzmann DJ, Snyder WB, Wendland B, Emr SD. Endosome-associated complex, ESCRT-II, recruits transport machinery for protein sorting at the multivesicular body. Dev Cell. 2002; 3:283–289. [PubMed: 12194858]
10. Hierro A, et al. Structure of the ESCRT-II endosomal trafficking complex. Nature. 2004; 431:221–225. [PubMed: 15329733]
11. Teo H, Perisic O, Gonzalez B, Williams RL. ESCRT-II, an endosome-associated complex required for protein sorting: Crystal structure and interactions with ESCRT-III and membranes. Dev Cell. 2004; 7:559–569. [PubMed: 15469844]

12. Im YJ, Hurley JH. Integrated structural model and membrane targeting mechanism of the human ESCRT-II complex. Dev Cell. 2008; 14:902–913. [PubMed: 18539118]
13. Kostelansky MS, et al. Structural and functional organization of the ESCRT-I trafficking complex. Cell. 2006; 125:113–126. [PubMed: 16615894]
14. Gill DJ, et al. Structural insight into the ESCRT-I/-II link and its role in MVB trafficking. Embo J. 2007; 26:600–612. [PubMed: 17215868]
15. Boura E, et al. Solution structure of the ESCRT-I and -II supercomplex: Implications for membrane budding and scission. Structure. 2012; 20:874–886. [PubMed: 22579254]
16. Wollert T, Hurley JH. Molecular mechanism of multivesicular body biogenesis by ESCRT complexes. Nature. 2010; 464:864–869. [PubMed: 20305637]
17. Carlson LA, Hurley JH. In vitro reconstitution of the ordered assembly of the endosomal sorting complex required for transport at membrane-bound HIV-1 Gag clusters. Proceedings of the National Academy of Sciences. 2012; 109:16928–16933.
18. Morita E, et al. Human ESCRT and ALIX proteins interact with proteins of the midbody and function in cytokinesis. EMBO J. 2007; 26:4215–4227. [PubMed: 17853893]
19. Morita E, et al. ESCRT-III Protein Requirements for HIV-1 Budding. Cell Host Microbe. 2011; 9:235–242. [PubMed: 21396898]
20. Goliand I, Nachmias D, Gershony O, Elia N. Inhibition of ESCRT-II-CHMP6 interactions impedes cytokinetic abscission and leads to cell death. Molecular Biology of the Cell. 2014; 25:3740–3748. [PubMed: 25232011]
21. Meng B, Ip NCY, Prestwood LJ, Abbink TEM, Lever AML. Evidence that the endosomal sorting complex required for transport-II (ESCRT-II) is required for efficient human immunodeficiency virus-1 (HIV-1) production. Retrovirology. 2015; 12:72. [PubMed: 26268989]
22. Christ L, et al. ALIX and ESCRT-I/II function as parallel ESCRT-III recruiters in cytokinetic abscission. J Cell Biol. 2016; 212:499–513. [PubMed: 26929449]
23. Tang S, et al. ESCRT-III activation by parallel action of ESCRT-I/II and ESCRT-0/Bro1 during MVB biogenesis. Elife. 2016
24. Cashikar AG, et al. Structure of cellular ESCRT-III spirals and their relationship to HIV budding. Elife. 2014:e02184. EM of ESCRT-III at HIV-1 Gag budding sites shows a funnel that nucleates at a narrow part of the membrane neck and widens as the funnel grows away from the bud.
25. Ladinsky MS, et al. Electron Tomography of HIV-1 Infection in GutAssociated Lymphoid Tissue. PLoS Path. 2014; 10
26. Rozycki B, Boura E, Hurley JH, Hummer G. Membrane-Elasticity Model of Coatless Vesicle Budding Induced by ESCRT Complexes. PLoS Comp Biol. 2012; 8
27. Mercker M, Marciniak-Czochra A. Bud-Neck Scaffolding as a Possible Driving Force in ESCRT-Induced Membrane Budding. Biophys J. 2015; 108:833–843. [PubMed: 25692588]
28. Teis D, Saksena S, Judson BL, Emr SD. ESCRT-II coordinates the assembly of ESCRT-III filaments for cargo sorting and multivesicular body vesicle formation. EMBO J. 2010; 29:871–883. [PubMed: 20134403]
29. Im YJ, Wollert T, Boura E, Hurley JH. Structure and Function of the ESCRT-II-III Interface in Multivesicular Body Biogenesis. Dev Cell. 2009; 17:234–243. [PubMed: 19686684]
30. Strack B, Calistri A, Craig S, Popova E, Gottlinger HG. AIP1/ALIX is a binding partner for HIV-1 p6 and EIAV p9 functioning in virus budding. Cell. 2003; 114:689–699. [PubMed: 14505569]
31. von Schwedler UK, et al. The protein network of HIV budding. Cell. 2003; 114:701–713. [PubMed: 14505570]
32. Kim J, et al. Structural basis for endosomal targeting by the Bro1 domain. Dev Cell. 2005; 8:937–947. [PubMed: 15935782]
33. Lee S, Joshi A, Nagashima K, Freed EO, Hurley JH. Structural basis for viral late-domain binding to Alix. Nat Struct Mol Biol. 2007; 14:194–199. [PubMed: 17277784]
34. Fisher RD, et al. Structural and biochemical studies of ALIX/AIP1 and its role in retrovirus budding. Cell. 2007; 128:841–852. [PubMed: 17350572]
35. Pires R, et al. A Crescent-Shaped ALIX Dimer Targets ESCRT-III CHMP4 Filaments. Structure. 2009; 17:843–856. [PubMed: 19523902]

36. McCullough J, Fisher RD, Whitby FG, Sundquist WI, Hill CP. ALIX-CHMP4 interactions in the human ESCRT pathway. Proc Natl Acad Sci U S A. 2008; 105:7687–7691. [PubMed: 18511562]
37. Dowlatshahi DP, et al. ALIX Is a Lys63-Specific Polyubiquitin Binding Protein that Functions in Retrovirus Budding. Dev Cell. 2012; 23:1247–1254. [PubMed: 23201121]
38. Keren-Kaplan T, et al. Structure-based in silico identification of ubiquitin-binding domains provides insights into the ALIX-V: ubiquitin complex and retrovirus budding. EMBO J. 2013; 32:538–551. [PubMed: 23361315]
39. Pashkova N, et al. The Yeast Alix Homolog Bro1 Functions as a Ubiquitin Receptor for Protein Sorting into Multivesicular Endosomes. Dev Cell. 2013; 25:520–533. [PubMed: 23726974]
40. Zhai QT, et al. Activation of the Retroviral Budding Factor ALIX. J Virol. 2011; 85:9222–9226. [PubMed: 21715492]
41. Ali N, et al. Recruitment of UBPY and ESCRT Exchange Drive HD-PTP-Dependent Sorting of EGFR to the MVB. Curr Biol. 2013; 23:453–461. [PubMed: 23477725]
42. Loncle N, Agromayor M, Martin-Serrano J, Williams DW. An ESCRT module is required for neuron pruning. Scientific Reports. 2015; 5
43. Parkinson MDJ, et al. A non-canonical ESCRT pathway, including histidine domain phosphotyrosine phosphatase (HD-PTP), is used for down-regulation of virally ubiquitinated MHC class I. Biochem J. 2015; 471:79–88. [PubMed: 26221024]
44. Muziol T, et al. Structural basis for budding by the ESCRT-III factor CHMP3. Dev Cell. 2006; 10:821–830. [PubMed: 16740483]
45. Tang S, et al. Structural basis for activation, assembly and membrane binding of ESCRT-III Snf7 filaments. Elife. 2015
46. Bajorek M, et al. Structural basis for ESCRT-III protein autoinhibition. Nat Struct Mol Biol. 2009; 16:754–762. [PubMed: 19525971]
47. Xiao JY, et al. Structural Basis of Ist1 Function and Ist1-Did2 Interaction in the Multivesicular Body Pathway and Cytokinesis. Molecular Biology of the Cell. 2009; 20:3514–3524. [PubMed: 19477918]
48. McCullough J, et al. Structure and membrane remodeling activity of ESCRT-III helical polymers. Science. 2015; 350:1548–1551. Atomic resolution structure of a CHMP1B: IST1 tube shows dramatic structural rearrangements in CHMP1B and, as a bonus, that this particular combination of ESCRTs carries out “normal” topology scission. [PubMed: 26634441]
49. Zamborlini A, et al. Release of autoinhibition converts ESCRT-III components into potent inhibitors of HIV-1 budding. Proc Natl Acad Sci U S A. 2006; 103:19140–19145. [PubMed: 17146056]
50. Shim S, Kimpler LA, Hanson PI. Structure/Function Analysis of Four Core ESCRT-III Proteins Reveals Common Regulatory Role for Extreme C-Terminal Domain. Traffic. 2007; 8:1068–1079. [PubMed: 17547705]
51. Lata S, et al. Structural Basis for Autoinhibition of ESCRT-III CHMP3. J Mol Biol. 2008; 378:818–827. [PubMed: 18395747]
52. Henne WM, Buchkovich NJ, Zhao Y, Emr SD. The Endosomal Sorting Complex ESCRT-II Mediates the Assembly and Architecture of ESCRT-III Helices. Cell. 2012; 151:356–371. [PubMed: 23063125]
53. Różycki B, Kim YC, Hummer G. SAXS Ensemble Refinement of ESCRT-III CHMP3 Conformational Transitions. Structure. 2011; 19:109–116. [PubMed: 21220121]
54. Schuh AL, et al. The VPS-20 subunit of the endosomal sorting complex ESCRT-III exhibits an open conformation in the absence of upstream activation. Biochem J. 2015; 466:625–637. [PubMed: 25588614]
55. Hanson PI, Roth R, Lin Y, Heuser JE. Plasma membrane deformation by circular arrays of ESCRT-III protein filaments. The Journal of Cell Biology. 2008; 180:389–402. [PubMed: 18209100]
56. Shen QT, et al. Structural analysis and modeling reveals new mechanisms governing ESCRT-III spiral filament assembly. The Journal of Cell Biology. 2014; 206:763–777. [PubMed: 25202029]
57. Chiaruttini N, et al. Relaxation of Loaded ESCRT-III Spiral Springs Drives Membrane Deformation. Cell. 2015; 163:866–879. Mechanical properties of ESCRTs are shown to be consistent with action as spiral springs. [PubMed: 26522593]

58. Lata S, et al. Helical Structures of ESCRT-III are Disassembled by VPS4. Science. 2008; 321:1354–1357. [PubMed: 18687924]
59. Effantin G, et al. ESCRT-III CHMP2A and CHMP3 form variable helical polymers in vitro and act synergistically during HIV-1 budding. Cell Microbiol. 2013; 15:213–226. [PubMed: 23051622]
60. Bodon G, et al. Charged Multivesicular Body Protein 2B (CHMP2B) of the Endosomal Sorting Complex Required for Transport-III (ESCRT-III) Polymerizes into Helical Structures Deforming the Plasma Membrane. J Biol Chem. 2011; 286:40276–40286. [PubMed: 21926173]
61. Allison R, et al. An ESCRT-spastin interaction promotes fission of recycling tubules from the endosome. J Cell Biol. 2013; 202:527–543. [PubMed: 23897888]
62. Dobro MJ, et al. Electron cryotomography of ESCRT assemblies and dividing Sulfolobus cells suggests that spiraling filaments are involved in membrane scission. Molecular Biology of the Cell. 2013; 24:2319–2327. [PubMed: 23761076]
63. Guizetti J, et al. Cortical constriction during abscission involves helices of ESCRT-III-dependent filaments. Science. 2011; 331:1616–1620. [PubMed: 21310966]
64. Baumgartel VBV, et al. Live-cell visualization of dynamics of HIV budding site interactions with an ESCRT component. Nat Cell Biol. 2011; 13:469–474. [PubMed: 21394086]
65. Jouvenet NJN, Zhadina M, Bieniasz PD, Simon SM. Dynamics of ESCRT protein recruitment during retroviral assembly. Nat Cell Biol. 2011; 13:394–401. [PubMed: 21394083]
66. Carlton JG, Martin-Serrano J. Parallels between cytokinesis and retroviral budding: a role for the ESCRT machinery. Science. 2007; 316:1908–1912. [PubMed: 17556548]
67. Agromayor M, Martin-Serrano J. Knowing when to cut and run: mechanisms that control cytokinetic abscission. Trends Cell Biol. 2013; 23:433–441. [PubMed: 23706391]
68. Elia N, Sougrat R, Spurlin T, Hurley JH, Lippincott-Schwartz J. Dynamics of ESCRT machinery during cytokinesis and its role in abscission. Proc Natl Acad Sci U S A. 2011; 108:4846–4851. [PubMed: 21383202]
69. Lee IH, Kai H, Carlson LA, Groves JT, Hurley JH. Negative membrane curvature catalyzes nucleation of endosomal sorting complex required for transport (ESCRT)-III assembly. Proc Natl Acad Sci U S A. 2015; 112:15892–15897. Real-time and super-resolution imaging of ESCRT-III polymerization on nanofabricated concave templates shows negative curvature preference for ESCRT-III nucleation. [PubMed: 26668364]
70. Teis D, Saksena S, Emr SD. Ordered Assembly of the ESCRT-III Complex on Endosomes Is Required to Sequester Cargo during MVB Formation. Dev Cell. 2008; 15:578–589. [PubMed: 18854142]
71. Babst M, Wendland B, Estepa EJ, Emr SD. The Vps4p AAA ATPase regulates membrane association of a Vps protein complex required for normal endosome function. EMBO J. 1998; 17:2982–2993. [PubMed: 9606181]
72. Monroe N, Hill CP. Meiotic Clade AAA ATPases: Protein Polymer Disassembly Machines. J Mol Biol. 2016; 428:1897–1911. [PubMed: 26555750]
73. Hurley JH, Yang D. MIT domainia. Dev Cell. 2008; 14:6–8. [PubMed: 18194647]
74. Monroe N, et al. The oligomeric state of the active Vps4 AAA ATPase. J Mol Biol. 2013; 426:510–525. [PubMed: 24161953]
75. Caillat C, et al. Asymmetric ring structure of Vps4 required for ESCRT-III disassembly. Nature Communications. 2015; 6 First structure of the active hexameric form of Vps4.
76. Obita T, et al. Structural basis for selective recognition of ESCRT-III by the AAA ATPase Vps4. Nature. 2007; 449:735–739. [PubMed: 17928861]
77. Stuchell-Brereton M, et al. ESCRT-III recognition by VPS4 ATPases. Nature. 2007; 449:740–744. [PubMed: 17928862]
78. Guo EZ, Xu Z. Distinct Mechanisms of Recognizing Endosomal Sorting Complex Required for Transport III (ESCRT-III) Protein IST1 by Different Microtubule Interacting and Trafficking (MIT) Domains. J Biol Chem. 2015; 290:8396–8408. [PubMed: 25657007]
79. Kieffer C, et al. Two distinct modes of ESCRT-III recognition are required for VPS4 functions in lysosomal protein targeting and HIV-1 budding. Dev Cell. 2008; 15:62–73. [PubMed: 18606141]

80. Shim S, Merrill SA, Hanson PI. Novel interactions of ESCRT-III with LIP5 and VPS4 and their implications for ESCRT-III disassembly. Mol Biol Cell. 2008; 19:2661–2672. [PubMed: 18385515]
81. Xiao J, et al. Structural basis of Vta1 function in the multi-vesicular body sorting pathway. Dev Cell. 2008; 14:37–49. [PubMed: 18194651]
82. Solomons J, et al. Structural basis for ESCRT-III CHMP3 recruitment of AMSH. Structure. 2011; 19:1149–1159. [PubMed: 21827950]
83. Merrill SA, Hanson PI. Activation of Human VPS4A by ESCRT-III Proteins Reveals Ability of Substrates to Relieve Enzyme Autoinhibition. J Biol Chem. 2010; 285:35428–35438. [PubMed: 20805225]
84. Norgan AP, et al. Relief of Autoinhibition Enhances Vta1 Activation of Vps4 via the Vps4 Stimulatory Element. J Biol Chem. 2013; 288:26147–26156. [PubMed: 23880759]
85. Davies BA, et al. Vps4 Stimulatory Element of the Cofactor Vta1 Contacts the ATPase Vps4 alpha 7 and alpha 9 to Stimulate ATP Hydrolysis. J Biol Chem. 2014; 289:28707–28718. [PubMed: 25164817]
86. Han H, et al. Binding of Substrates to the Central Pore of the Vps4 ATPase Is Autoinhibited by the Microtubule Interacting and Trafficking (MIT) Domain and Activated by MIT Interacting Motifs (MIMs). J Biol Chem. 2015; 290:13490–13499. [PubMed: 25833946]
87. Scott A, et al. Structural and mechanistic studies of VPS4 proteins. EMBO J. 2005; 24:3658–3669. [PubMed: 16193069]
88. Gonciarz MD, et al. Biochemical and Structural Studies of Yeast Vps4 Oligomerization. J Mol Biol. 2008; 384:878–895. [PubMed: 18929572]
89. Hartmann C, et al. Vacuolar protein sorting: Two different functional states of the AAA-ATPase Vps4p. J Mol Biol. 2008; 377:352–363. [PubMed: 18272179]
90. Yu ZH, Gonciarz MD, Sundquist WI, Hill CP, Jensen GJ. Cryo-EM structure of dodecameric Vps4p and its 2 : 1 complex with Vta1p. J Mol Biol. 2008; 377:364–377. [PubMed: 18280501]
91. Landsberg MJ, Vajjhala PR, Rothnagel R, Munn AL, Hankamer B. Three-Dimensional Structure of AAA ATPase Vps4: Advancing Structural Insights into the Mechanisms of Endosomal Sorting and Enveloped Virus Budding. Structure. 2009; 17:427–437. [PubMed: 19278657]
92. Yang B, Stjepanovic G, Shen QT, Martin A, Hurley JH. Vps4 disassembles an ESCRT-III filament by global unfolding and processive translocation. Nat Struct Mol Biol. 2015; 22:492–498. Shows that Vps4 disassembles ESCRT-III by unfolding the subunits and pulling them through the central pore. [PubMed: 25938660]
93. Azmi IF, et al. ESCRT-III family members stimulate Vps4 ATPase activity directly or via Vta1. Dev Cell. 2008; 14:50–61. [PubMed: 18194652]
94. Yang D, Hurley JH. Structural role of the Vps4-Vta1 interface in ESCRT-III recycling. Structure. 2010; 18:976–984. [PubMed: 20696398]
95. Fabrikant G, et al. Computational Model of Membrane Fission Catalyzed by ESCRT-III. PLoS Comput Biol. 2009; 5:e1000575. [PubMed: 19936052]
96. Wollert T, Wunder C, Lippincott-Schwartz J, Hurley JH. Membrane scission by the ESCRT-III complex. Nature. 2009; 458:172–177. [PubMed: 19234443]
97. Van Engelenburg SB, et al. Distribution of ESCRT Machinery at HIV Assembly Sites Reveals Virus Scaffolding of ESCRT Subunits. Science. 2014; 343:653–656. [PubMed: 24436186]
98. Prescher J, et al. Super-resolution imaging of ESCRT-proteins at HIV-1 assembly sites. PLoS Path. 2015; 11
99. Henne WM, Buchkovich NJ, Emr SD. The ESCRT pathway. Dev Cell. 2011; 21:77–91. [PubMed: 21763610]
100. Hurley JH, Hanson PI. Membrane budding and scission by the ESCRT machinery: it's all in the neck. Nat Rev Mol Cell Biol. 2010; 11:556–566. [PubMed: 20588296]
101. McCullough J, Colf LA, Sundquist WI. Membrane Fission Reactions of the Mammalian ESCRT Pathway. Annu Rev Biochem. 2013; 82:663–692. [PubMed: 23527693]
102. Lenz M, Crow DJG, Joanny JF. Membrane Buckling Induced by Curved Filaments. Phys Rev Lett. 2009; 103

103. Carlson LA, Shen QT, Pavlin MR, Hurley JH. ESCRT Filaments as Spiral Springs. Dev Cell. 2015; 35:397–398. [PubMed: 26609952]

104. Schekman R, Orci L. Coat proteins and vesicle budding. Science. 1996; 271:1526–1533. [PubMed: 8599108]

105. Bonifacino JS, Glick BS. The mechanisms of vesicle budding and fusion. Cell. 2004; 116:153–166. [PubMed: 14744428]

106. Nickerson DP, Russell DW, Odorizzi G. A concentric circle model of multivesicular body cargo sorting. EMBO Rep. 2007; 8:644–650. [PubMed: 17603537]

107. Odorizzi G. Membrane manipulations by the ESCRT machinery. F1000Research. 2015; 4:516–516. [PubMed: 26339479]

108. Vietri M, et al. Spastin and ESCRT-III coordinates mitotic spindle disassembly and nuclear envelope resealing. Nature. 2015; 522:231–235. [PubMed: 26040712]

109. Zhai Q, et al. Structural and functional studies of ALIX interactions with YPXnL late domains of HIV-1 and EIAV. Nat Struct Mol Biol. 2008; 15:43–49. [PubMed: 18066081]

On line summary

- ESCRTs carry out scission of membrane necks with a topology (or sidedness) opposite to the better-understood process carried out by coat proteins, dynamin, and BAR domain proteins
- ESCRT membrane scission is initiated by two upstream branches: the first, comprising ESCRT-I and –II, and the second comprising ALIX.
- ESCRT-III proteins comprise a family of 12 different subunits in humans. ESCRT-III monomers are about 200 amino acids and have open and closed conformations.
- ESCRT-III proteins can assemble into flat spirals, helical tubes, or conical funnels.
- ESCRT-III assemblies are taken apart by the AAA+ ATPase Vps4, which unfolds ESCRT-III monomers and threads them through a central pore
- It is currently unresolved whether scission is mediated by the drawing-together of membrane necks by a tapered dome, buckling by the mechanical spring-like action of curved ESCRT filaments, or some other means.

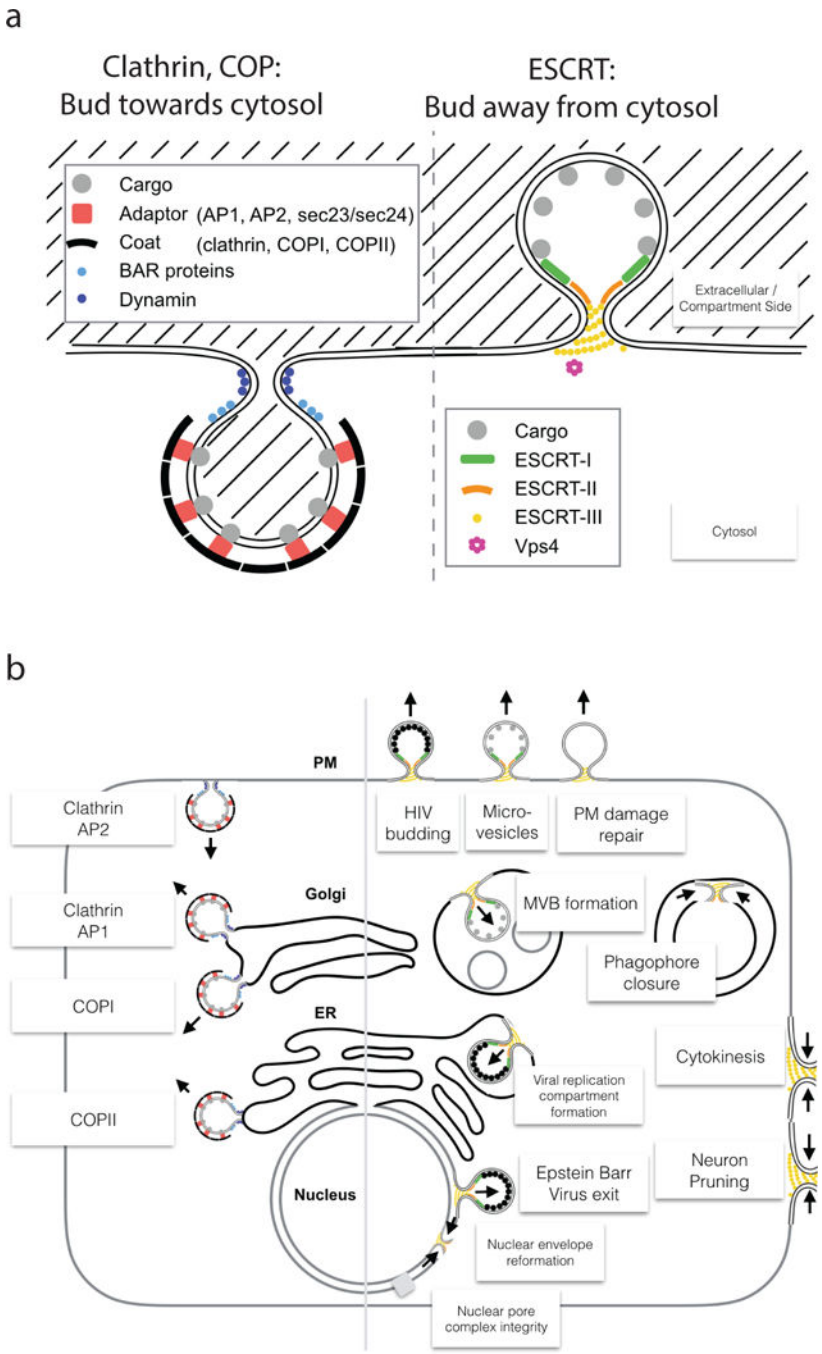

Figure 1. Reverse topology membrane scission

a| "Normal" and "reverse" topology membrane scission: "Normal" scission such as occurs in clathrin and coated vesicle biogenesis, whereas "reverse" scission carried out by ESCRTs acts in vesicle budding away from the cytosol. Note that a fundamental difference arises from only the cytosolic membrane side being accessible for protein scaffolding and scission machinery. **b**| Functions of the ESCRT pathway (right) compared with "normal" scission functions (left). Clathrin, COPI, and COPII are vesicle coats, while AP-1 and AP-2 are adaptor complexes that connect clathrin to membranes and vesicular cargo.

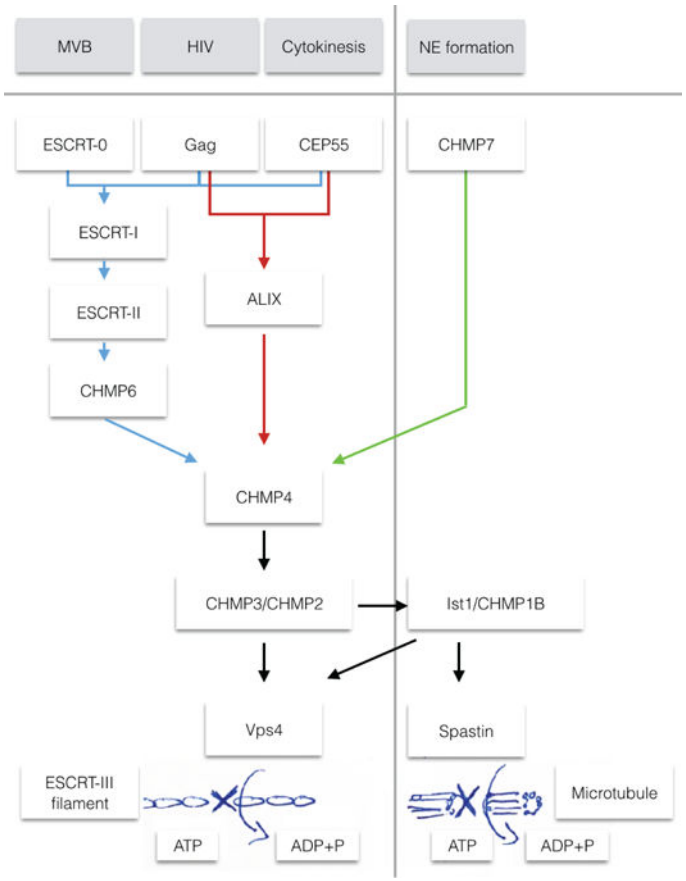

Figure 2. Organization of the ESCRT system

Schematic of the three branches of the ESCRT pathway, explored in the four functions of multivesicular body (MVB) genesis, HIV budding, Cytokinesis and nuclear envelope (NE) formation. The first three of these functions can all use the 'classic' pathway (ESCRT-I, ESCRT-II, CHMP6), whereas HIV budding and cytokinesis have respective adaptors that can use ALIX to bridge directly to CHMP4[22]. In NE formation, CHMP7 functions as the bridge to CHMP4[108]. From CHMP4, the canonical pathway uses CHMP2 and CHMP3 that recruit Vps4 for eventual disassembly of the ESCRT filaments. In NE formation, the ESCRT protein IST1 is required, which in turn recruits the microtubule severing enzyme spastin[108].

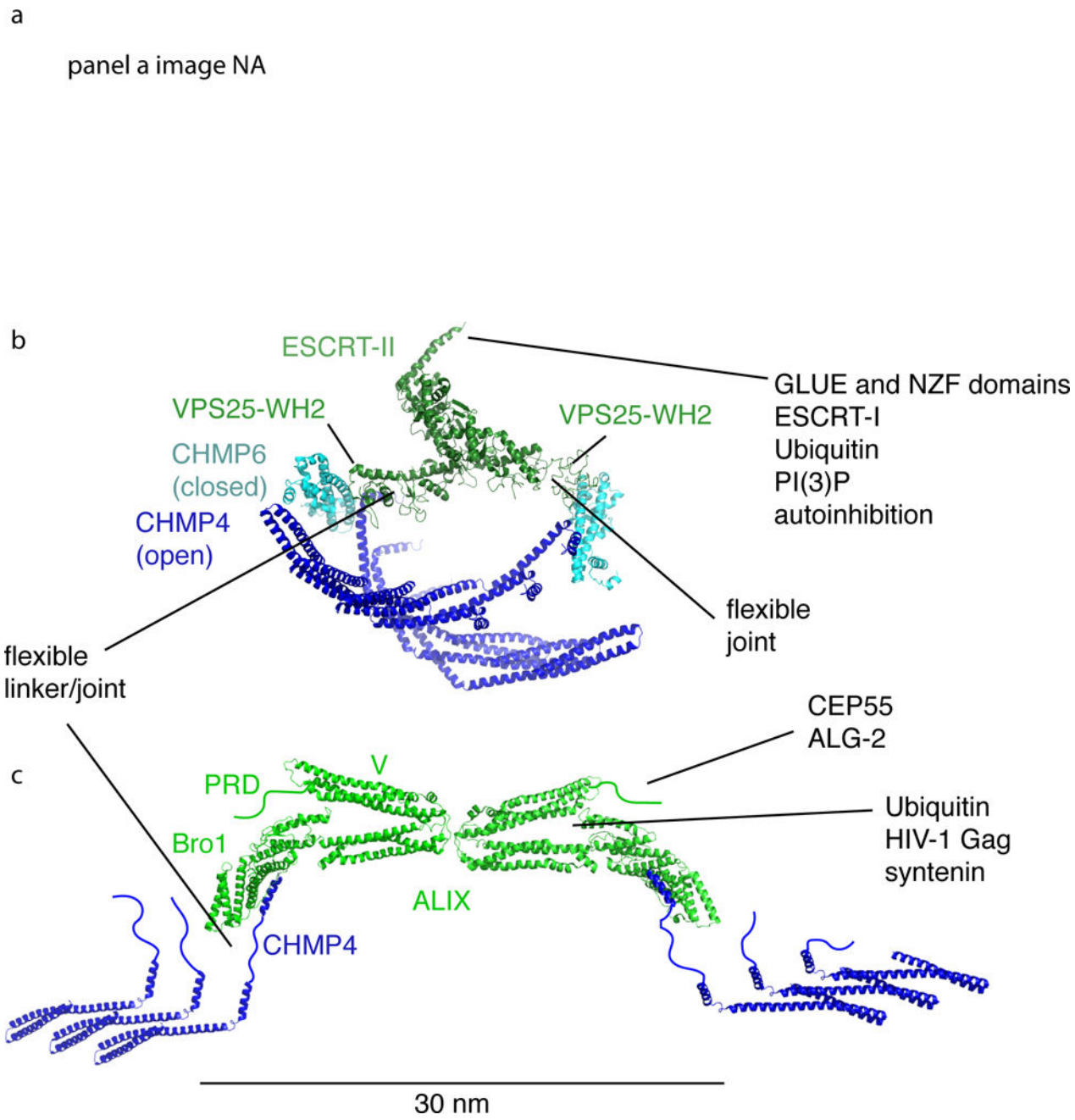

Figure 3. The ESCRT-I/II and ALIX branches of the upstream ESCRTs

In nearly every context in which the ESCRTs occur, the upstream components recruit, activate, and organize the polymerization of ESCRT-III. The only exception is in reformation and quality control of the NE, the role of ESCRT-II is apparently replaced by CHMP7. This figure shows how the upstream elements ESCRT-I/II and ALIX organize ESCRT-III at the nanoscale (**a**) and atomic scales (**b** and **c**). **a**| Struts of putative ESCRT-I/II complexes imaged at a HIV-1 Gag budding site by DEEM (reprinted with permission[24]) (this panel not in NIHMS version due to third party rights). **b**| ESCRT-II (green) initiates two CHMP4 filaments (blue) via CHMP6 (teal). Structures shown are from RCSB entries 1U5T[10],

3HTU[29], and 3JCI[48]. The structures of polymerized IST1 and CHMP1B are used as stand-ins for the CHMP6:CHMP4 complex, whose structure is not known. **c**| A dimer of ALIX (green) initiates two CHMP4 filaments (blue) via direct interactions with the C-terminus of CHMP4. Structures shown are from RCSB entries 2OEV[34], 3C3O[109], and 5FD7[45].

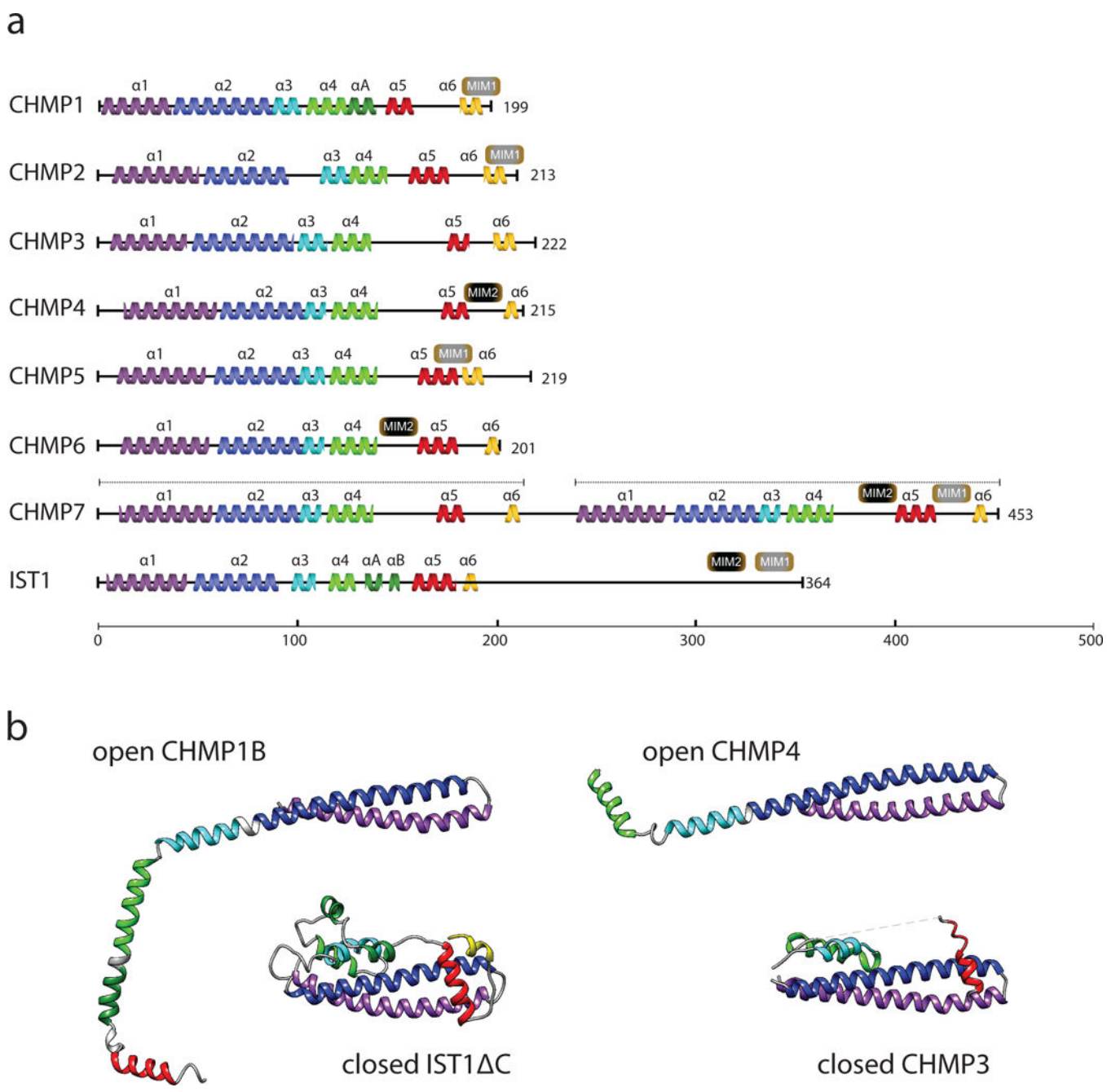

Figure 4. The ESCRT-III proteins

a| Primary structural organization of the 12 human ESCRT-III proteins. Yeast Snf7 (CHMP4), CHMP2B and CHMP1B are depicted as representatives of the CHMP4A-C, CHMP2A-B, and CHMP1A-B families. The main structural helices are colored: α1 (purple), α2 (blue), α3 (cyan), α4 (green), αA (dark green), αB (dark green), autoinhibitory helix α5 (red) and interaction helix α6 (yellow). The C-termini of ESCRT-IIIs carry microtubule-interacting and transport (MIT)-interacting motifs (MIM1, MIM2) that are responsible for binding to other components of the ESCRT pathway, such as Vps4. **b**| Crystal structures of ESCRT-III monomers. Color coding same as a. CHMP1B and CHMP4

have both been found to adopt open conformations, with helices α2 and α3 merging[45, 48]. Ist1ΔC and CHMP3 are shown in the closed conformations in which they have been crystallized[44, 46].

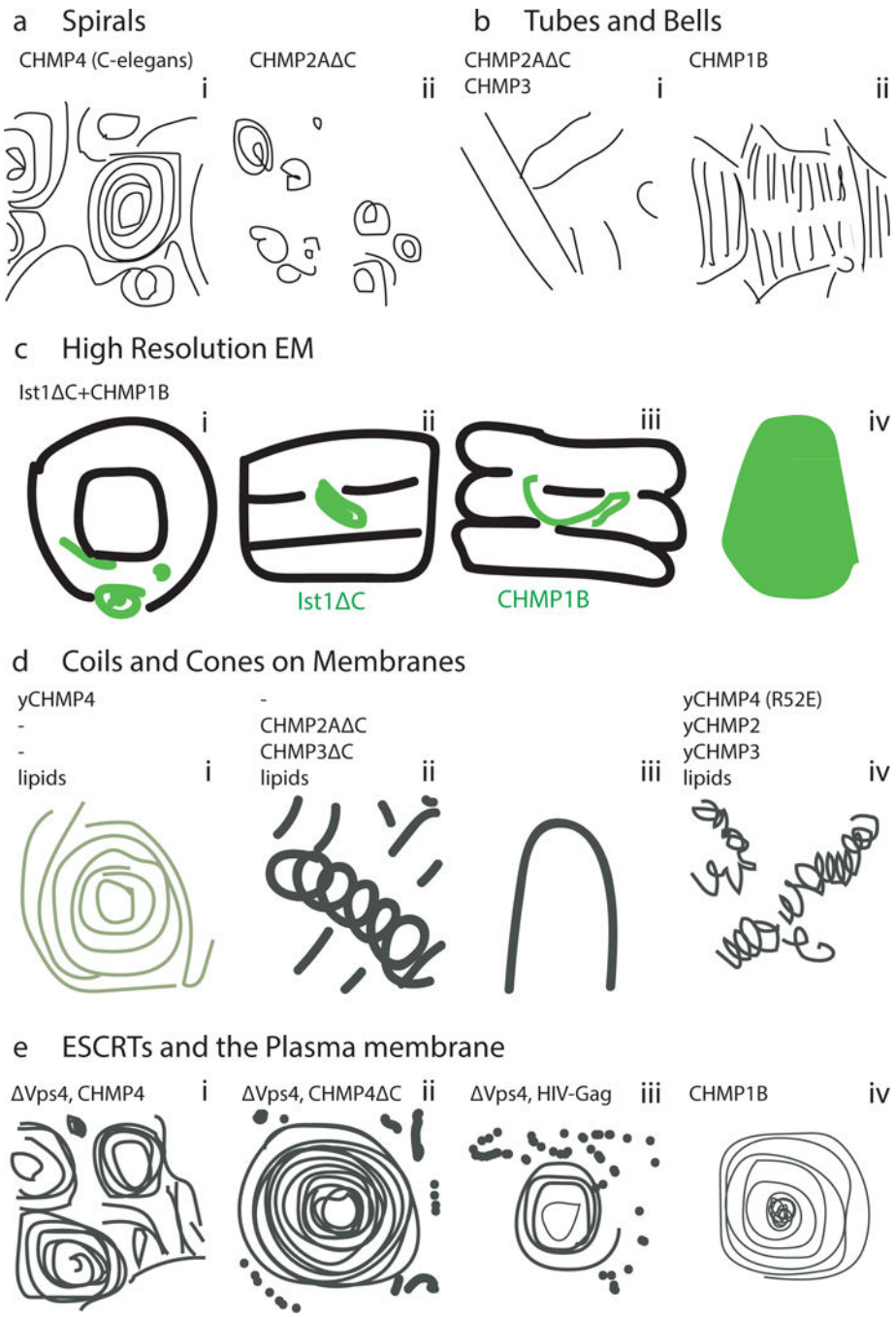

Figure 5. ESCRT-III assembly structures

a| Spirals. i) Cryo-EM of *C. elegans* CHMP4[56]. ii) Negative-stain EM of CHMP2AΔC polymers[59]. Scale bar: 40nm**. b**| Tubes and bell shapes. i) Cryo-EM of CHMP2AΔC–CHMP3 tubes with cones (*) and tubes (^)[59]. Scale bar: 40nm. ii) Cryo-EM of CHMP1B[62]. **c**| Cryo-EM structure of ESCRT-III tubular assembly. i) End-on view of IST1ΔC-CHMP1B tube with IST1ΔC in light green and CHMP1B in dark green[48]. ii) External view of the reconstructed helix with IST1ΔC highlighted[48]. iii) Cutaway view with CHMP1B highlighted[48]. iv) Side view of an IST1ΔC-CHMP1B cone[48]. Scale bar: 5.1nm. **d**| EM of

ESCRT-III assemblies on membranes. i) TEM of a single Snf7 spiral on a POPC:POPS membrane[57]. ii) CHMP2AΔC-CHMP3ΔC tubes in the presence of SOPC:DOPS[58]. Tube diameter ~55nm. iv) $Snf7_{R52E}$:Vps24:Vps2 2:1:1 helices assembled on POPC:POPC:PI(3)P monolayers[52]. **e**| EM of ESCRT-III in cells. i) Anaglyph of plasma membranes from COS-7 cells expressing CHMP4A[24]. Scale bar: 100nm. ii) Filament spirals on COS-7 cell membranes expressing $CHMP4A_{1-164}$. Scale bar: 100nm[48]. iii) HEK293T cells treated with Vps4A & Vps4B siRNA accumulate filament-encircled Gag assemblies[24]. Scale bar: 100nm. iv) Spirals on COS-7 cells expressing FLAG-CHMP1B[48]. Scale bar: 50nm. (this figure not included in NIHMS version due to third party rights)

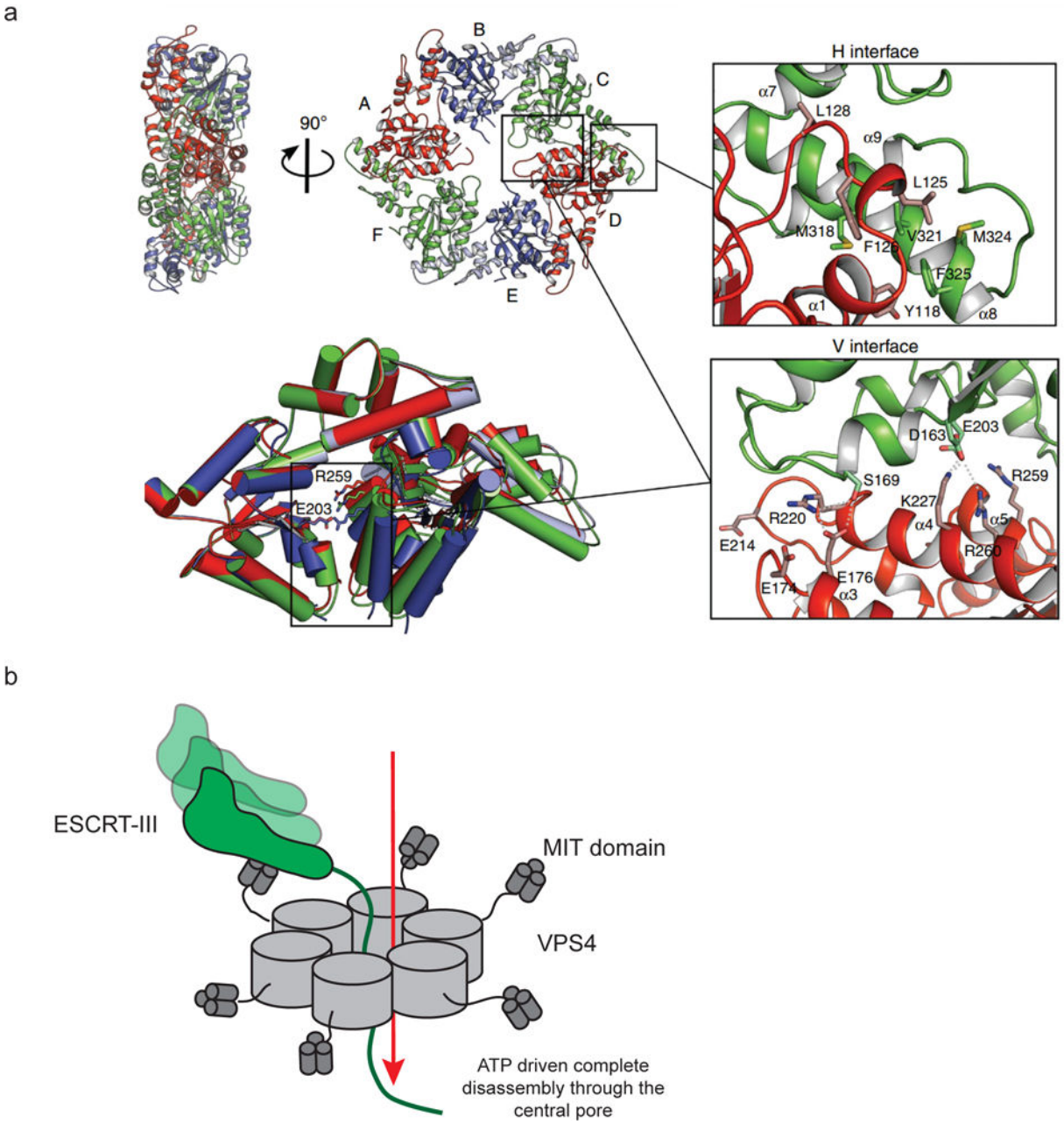

Figure 6. ESCRT complex disassembly

a| The structure of MsVps4 shows how pore structure, nucleotide binding, and hexamerization are interconnected. Crystal structure of the MsVps4ΔMIT pseudohexamer viewed from two orientations[75]. The protomers are labeled from A to F and identical protomers are represented in the same color, except for protomers B and E, whose small ATPase domain is shown in light blue and the large ATPase domain in dark blue. Superposition of the three different dimers present in the pseudohexamer and molecular interactions at the two different interfaces are shown. **b**| VPS4 hexamers completely disassemble target ESCRT-III subunits by disassembling them through the central pore[92].

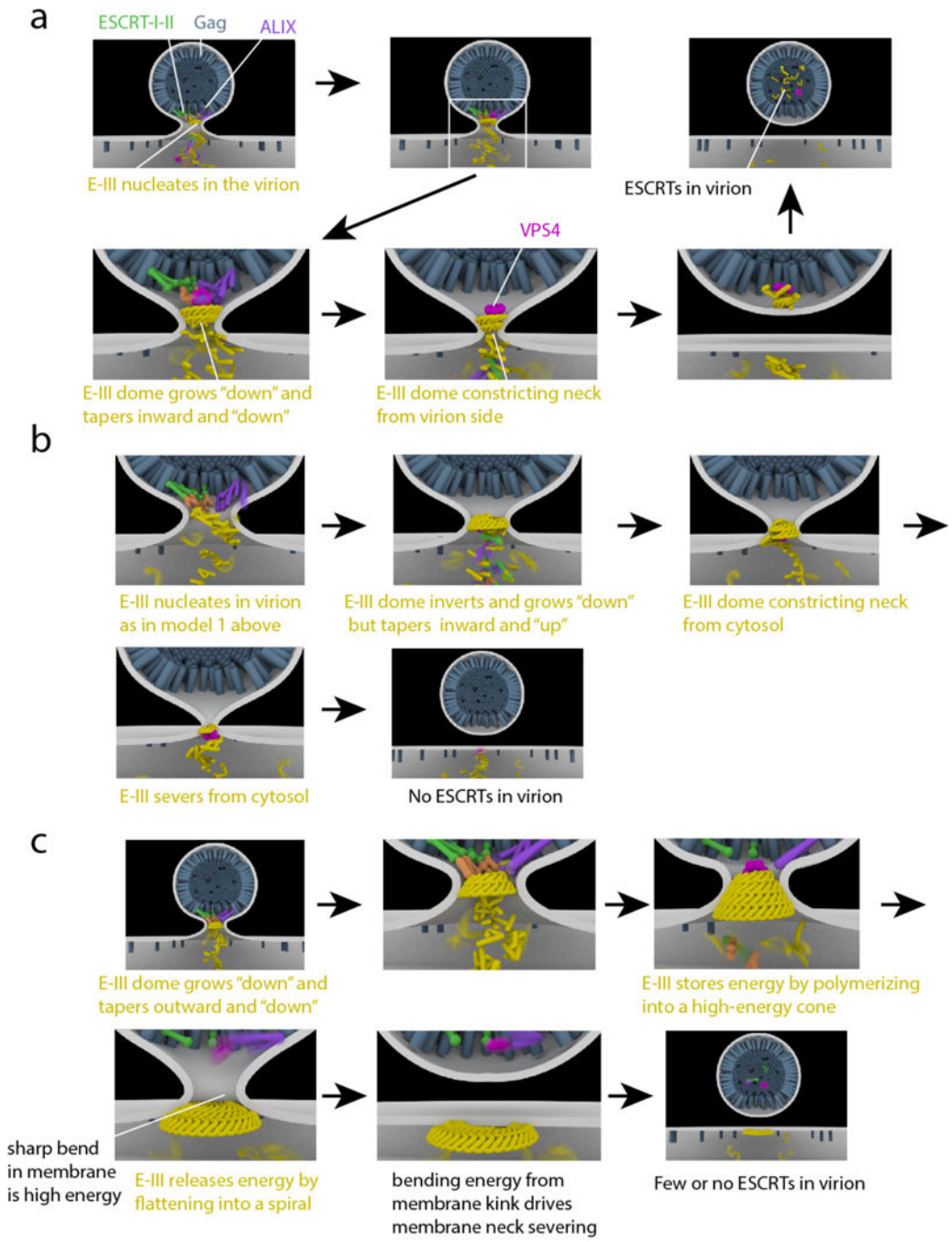

Figure 7. Models for ESCRT-mediated scission

HIV-1 Gag (blue) accumulates at the membrane (white), causing initial membrane deformation. ESCRT-I/ESCRT-II (green/orange) and ALIX (purple) are recruited by Gag. ESCRT-III (yellow) is recruited by ESCRT-II and ALIX, and polymerizes in the bud neck. **a**| "Original" dome model. ESCRT-III polymerizes away from the virion and towards the cytosol whilst forming consecutively narrower rings such that the dome tapers to a point in the same direction in which it grows. VPS4 (pink) depolymerizes ESCRT-III and scission occurs. ESCRTs are retained in the virion. **b**| Reverse dome model. ESCRTs are released to

the cytosol. As compared to the “original” dome model (**a**), ESCRT-III grows in the same direction, but tapers in the opposite direction. It is not clear how this paradoxical mode of growth could occur in practice, but it would presumably require active remodeling by VPS4. **c**| Buckling model. As in the reverse dome model (**b**), ESCRTs are released to the cytosol at the end. ESCRT-III polymerizes outward from the virion towards the cytosol, with consecutive wider rings. The cone is higher in energy than a flat spiral. Conversion of the cone to a spiral releases the tension, but at the cost of creating sharp bends where the virion is attached to the plasma membrane. The high energy of these bends is released when the virion is severed.